GEOPHYSICS, VOL. 62, NO. 2 (MARCH-APRIL 1997); P. 630–643, 12 FIGS., 1 TABLE.

Data-matrix asymmetry and polarization changes from multicomponent surface seismics

Xiang-Yang Li* and Colin MacBeth*

ABSTRACT

We present methods for interpreting data-matrix asymmetry and polarization changes with depth from multicomponent surface seismics. There are two main sources of data matrix asymmetry in four component shear-wave seismics: that arising from the acquisition geometry caused by source and receiver misorientation, misalignment, imbalance, and cross-coupling, and that arising from the medium caused by variations in the geological structure, lithology, or stress. The asymmetry caused by acquisition geometry is more significant than that from the medium. Two asymmetry indices are used to quantify these medium and acquisition asymmetries separately. Their behavior may be used to identify the origin of the asymmetry.

The asymmetry caused by the medium is studied by deriving approximate normal-incidence, plane-wave reflection coefficients for an interface separating two anisotropic media with differently oriented symmetry axes. The degree of asymmetry in the reflectivity is proportional to the product of the degree of anisotropy in the layers above and below the reflector, and is thus small for most realistic cases. Consequently, the reflection coefficients can be approximated by a similarity transform of the principal reflection coefficients using the expected polarization difference. These equations can then be used to formulate a singular-value decomposition (SVD) in the time-domain to recover both the principal reflectivity and the changes of polarizations with depth. Applications to field data in south Texas reveal the potential of the technique, and zones of polarization changes in the Austin Chalk are identified that may be correlated with fracture swarms.

INTRODUCTION

Shear-wave splitting (birefringence) in multicomponent seismic data has excited considerable interest because of the possibility to use this phenomenon to characterize the internal pore-crack geometry and the local stress field of reservoir rocks. The polarization direction of the leading split shear wave may give information about the orientation of in-situ stresses, and these stresses strongly affect several reservoir characteristics related to drilling, simulation and production (Bruno and Winterstein, 1994). In recent years, many processing techniques have been developed to estimate and interpret this polarization azimuth from recorded multicomponent seismic data (e.g., Alford, 1986; Thomsen, 1988; Winterstein and Meadows, 1991; Li and Crampin, 1993a; Lefeuvre et al., 1992; Zeng and MacBeth, 1993a, b; MacBeth et al., 1994). The polarization azimuth of the leading split shear wave, as related to the direction of the maximum in-situ stress, may vary both laterally with structural location and vertically with depth due to material properties, stratigraphy, bedding, and faults (Warpinski and Teufel, 1991). This has been observed in both multicomponent seismic reflection data (Squires et al., 1989; Lewis et al., 1991), and vertical seismic profiles (VSPs) (Winterstein and Meadows, 1991). Although most processing techniques designed for multicomponent VSPs have taken into account polarization changes (e.g., Winterstein and Meadows, 1991; Lefeuvre et al., 1992; Zeng and MacBeth, 1993a), those designed for multicomponent seismic reflection data often assume constant polarization direction (e.g., Alford, 1986; Thomsen, 1988; Li and Crampin, 1993a).

Common field practice in acquiring multicomponent shear-wave data often employs two horizontal sources and two horizontal receivers; the recorded data thus contains four components arranged in a 2×2 data matrix. The VSP data matrix recorded in the borehole generally has a higher signal-to-noise ratio than the reflection data matrix recorded on the free surface, and is less problematic for anisotropic analysis.

Presented at the 65th Annual International Meeting, Society of Exploration Geophysicists. Manuscript received by the Editor June 19, 1995; revised manuscript received May 6, 1996.
*Edinburgh Anisotropy Project, British Geological Survey, Murchison House, West Mains Road, Edinburgh EH9 3LA, United Kingdom.

The reciprocal up- and down-going raypaths for surface seismic data also make the determination of polarization changes more difficult than the one-way transmission response for VSP. However, there is a growing need for correctly predicting reservoir properties away from boreholes, between boreholes, or even before drilling, to improve reservoir recovery efficiency. These requirements stimulate the current work in this area to determine a scheme for detecting polarization changes from surface-seismic reflection data. To achieve this aim, we must contend with factors related to poor experiment control, such as source strength, balance, and misorientation, and geophone sensitivity, coupling, and misorientation, as well as other acquisition conditions and near-surface effects. As it is almost impossible to isolate all these factors in the reflection data matrix, we focus on factors that directly influence the *relative* variation of particle displacements for different wavetypes. In particular, as demonstrated in MacBeth et al. (1994), the presence or absence of symmetry between the off-diagonal elements in a VSP-data matrix is a basic indicator of the presence or absence of anisotropy and source and geophone misorientation, in addition to polarization changes with depth. Here, we extend this methodology to the reflection data matrix, and examine the viability of the asymmetry concept for our case.

Our approach is to represent all factors affecting the data matrix by three matrix functions for the source, geophone, and medium response in a vector convolutional model. Through this, we introduce the concept of data matrix asymmetry and examine the behavior of asymmetry indicators with changes in acquisition and medium parameters. Next, we demonstrate that such asymmetry indicators are useful in separating these two categories of effect. After identification, a singular value decomposition (SVD) may then be applied to separate the shear waves and recover the changes in polarization azimuth at each reflector. This approach is illustrated using both synthetic and field data.

MEASURING DATA MATRIX ASYMMETRY

Vector convolutional model

We consider a four-component shear-wave survey with two horizontal sources and two horizontal receivers (Alford, 1986), forming a data matrix of traces $\underset{\sim}{\mathbf{d}}(t)$:

$$\underset{\sim}{\mathbf{d}}(t) = \begin{bmatrix} xx(t) & yx(t) \\ xy(t) & yy(t) \end{bmatrix}, \tag{1}$$

where the top row, $xx(t)$ and $yx(t)$, are the in-line (x-axis) traces from the in-line and cross-line sources, respectively, and the bottom row, $xy(t)$ and $yy(t)$, are the cross-line (y-axis) traces from the in-line and cross-line sources, respectively. We also introduce $\underset{\sim}{\mathbf{D}}(\omega)$ as the Fourier transform of $\underset{\sim}{\mathbf{d}}(t)$ such that:

$$\underset{\sim}{\mathbf{D}}(\omega) = \begin{bmatrix} XX(\omega) & YX(\omega) \\ XY(\omega) & YY(\omega) \end{bmatrix}, \tag{2}$$

where ω is the angular frequency, the symbols in upper case represent variables in the frequency domain. The symbols in lower case represent corresponding variables in the time domain. Assuming the Earth is a linear system for seismic waves satisfying the convolution model (Zeng and MacBeth, 1993a, b), we have, in the frequency domain:

$$\underset{\sim}{\mathbf{D}}(\omega) = \underset{\sim}{\mathbf{G}}(\omega)\underset{\sim}{\mathbf{M}}(\omega)\underset{\sim}{\mathbf{S}}(\omega), \tag{3}$$

where $\underset{\sim}{\mathbf{S}}(\omega)$ is the source signature, $\underset{\sim}{\mathbf{G}}(\omega)$ is the geophone response, and $\underset{\sim}{\mathbf{M}}(\omega)$ is the medium response for the two shear modes $qS1$ and $qS2$. After proper compensation for the source signature and geophone response by multicomponent amplitude corrections (Li, 1994), we can obtain $\underset{\sim}{\mathbf{M}}(\omega)$ from $\underset{\sim}{\mathbf{D}}(\omega)$. Thus in the rest of the paper, $\underset{\sim}{\mathbf{D}}(\omega)$ will be assumed as $\underset{\sim}{\mathbf{M}}(\omega)$ with source and geophone compensation applied, unless otherwise specified.

Asymmetry definition and indices $\gamma(\tau)$ and $\Delta\theta(\tau)$

Mathematically, a matrix is defined as asymmetric if the off-diagonal elements of the matrix are unequal:

$$\underset{\sim}{\mathbf{d}}(t) \neq \underset{\sim}{\mathbf{d}}^T(t); \qquad \underset{\sim}{\mathbf{D}}(\omega) \neq \underset{\sim}{\mathbf{D}}^T(\omega), \tag{4}$$

where superscript T denotes the transpose operator. In real seismic data, because of the presence of noise and the limited bandwidth of the seismic signals, an instantaneous definition of asymmetry clearly will not yield any useful insights into the data matrix. Thus the asymmetry of the data matrix must be defined over a time window, based on the similarity of the off-diagonal elements of the data matrix. This measure must be robust in the presence of noise; ideally, it may also reveal the underlying cause of the asymmetry, that is, whether it is caused by abnormal acquisition conditions or by complications in the medium properties such as anisotropy or inhomogeneity. Introducing two linear transforms in the time domain, following Li and Crampin (1993a):

$$\begin{bmatrix} \zeta(t) \\ \chi(t) \end{bmatrix} = \begin{bmatrix} xx(t) + yy(t) \\ xy(t) - yx(t) \end{bmatrix}. \tag{5}$$

$\zeta(t)$ and $\chi(t)$ define transformed time series. We form a vector in the plane of (ζ, χ), with $\chi(t)$ being related directly to the instantaneous asymmetry of the data matrix. Two window-based indices can now be defined as

$$\gamma(\tau) = \frac{\lambda_{\text{minor}}}{\lambda_{\text{major}}} \tag{6}$$

and

$$\Delta\theta(\tau) = \frac{1}{2}\tan^{-1}\left[\frac{2|\sum_t \chi(t+\tau)\zeta(t+\tau)|}{|\sum_t [\chi^2(t+\tau) - \zeta^2(t+\tau)]|}\right], \tag{7}$$

where λ_{minor} and λ_{major} are the minor and major eigenvalues of the covariance matrix $\underset{\sim}{\mathbf{B}}(\tau)$ for $\zeta(t)$ and $\chi(t)$ (Kanasewich 1981):

$$\underset{\sim}{\mathbf{B}}(\tau) = \begin{bmatrix} \sum_t \zeta^2(t+\tau) & \sum_t \zeta(t+\tau)\chi(t+\tau) \\ \sum_t \zeta(t+\tau)\chi(t+\tau) & \sum_t \chi^2(t+\tau) \end{bmatrix}. \tag{8}$$

The summation is over a sliding time window, and τ represents the beginning of the window. The covariance matrix $\underset{\sim}{\mathbf{B}}(\tau)$ is a real symmetric matrix and has two eigenvalues (λ_{minor} and λ_{major}); $\lambda_{\text{minor}} = 0$ if and only if the determinant of $\underset{\sim}{\mathbf{B}}(\tau)$ is

zero, implying that $\zeta(t)$ and $\chi(t)$ are linearly dependent on each other. As defined in equation (7), $\Delta\theta(\tau)$ is the Jacobi rotation angle required to diagonalize the covariance $\underset{\sim}{\mathbf{B}}(\tau)$. The data matrix $\underset{\sim}{\mathbf{d}}(t)$ is said to be symmetric if $\gamma(\tau)$ is zero for any given τ, or asymmetric if $\gamma(\tau)$ is nonzero for any given τ (a larger $\gamma(\tau)$ implies a greater degree of asymmetry). The reasons for this definition and the physical significance of $\Delta\theta(\tau)$ are discussed below.

Significance of $\gamma(\tau)$ and $\Delta\theta(\tau)$

Here, $\zeta(t)$ and $\chi(t)$ describe a position vector, the coordinate (ζ, χ) being defined by the temporal trajectory in the displacement plane (Figure 1). The major and minor eigenvalues of the covariance matrix of the two coordinates represent the major and minor axis of the motion in this diagram (Kanasewich, 1981). If the motion is nearly linear (Figure 1a), the length of the minor axis (the minor eigenvalue), is very small compared with the major one, and $\gamma(\tau)$ is also small. If the motion is elliptical (Figure 1b), the length of the minor axes is comparable to the major axis and $\gamma(\tau)$ is nonzero. Thus $\gamma(\tau)$ is a measure of the linearity of the transformed displacement vector $[\zeta(t), \chi(t)]$. If we rotate the ζ and χ axes, the minor and the major axis of the particle motion and hence $\gamma(\tau)$ will not change (Figure 1). Thus, $\gamma(\tau)$ is always independent of the coordinate frame. For linearly polarized motion, there will always exist a coordinate transform which maximizes ζ and minimizes χ (Figure 1a) or vice versa, hence leading to a symmetric data matrix. This is why we use the degree of nonlinearity to define the degree of asymmetry. Index $\Delta\theta(\tau)$ is the least-square measurement of the angle between the major axis and the axis ζ in the transform plane (ζ, χ), as shown in Figure 1a. Thus, $\Delta\theta(\tau)$ is the optimal rotation angle required to maximize one axis and minimize the other or, alternatively, the angle that makes the data matrix symmetric in an optimal sense. These indices show that the concept of data matrix asymmetry is linked to the nonlinearity of the polarization defined in this transform domain. We may draw an analogy between the preservation of the source polarization in an isotropic medium and the preservation of linearity in this transform domain, as departure from either may infer inhomogeneity.

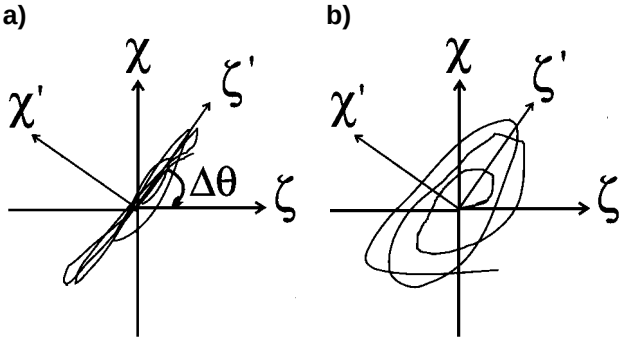

FIG. 1. (a) A linearly polarized motion; (b) an elliptically polarized motion. ζ and χ represent the transform plane coordinates; with ζ' and χ' the coordinate system along the major and minor axes after rotation.

INTERPRETING DATA MATRIX ASYMMETRY

Source and geophone misorientation and differential coupling because of interactions with the near surface can all cause asymmetry in the acquisition terms of equation (3), and so too can lateral variations and depth changes in the anisotropy orientation. It has been shown that it is possible to distinguish among certain acquisition errors such as misorientation, polarity reversal, and also polarization changes using asymmetry in multicomponent VSPs (MacBeth et al., 1994). In surface seismics, the asymmetry indices respond differently, so that we cannot carry forward these results. We investigate two categories of effect: source and geophone misorientation, and polarization change with depth on the asymmetry indices. In the latter case, we examine the reflectivity response in the presence of a depth change in polarization.

Source and geophone misorientation

Here, we consider two quasi–shear waves propagating in an anisotropic medium, for which mode conversion and cross-coupling may be simply related to a rotational transformation of a nondiagonal propagator matrix. If the orthogonal source and geophone sets are not oriented along the same directions, as shown in Figure 2, where the in-line source is assumed to be at an angle α_S and the in-line geophone at an angle α_G to the polarization direction of the fast shear wave ($qS1$), the data matrix $\underset{\sim}{\mathbf{D}}(\omega)$ may be written (after correcting for source signature and geophone response) as

$$\underset{\sim}{\mathbf{D}}(\omega) = \underset{\sim}{\mathbf{C}}(\alpha_G)\begin{bmatrix} QS1(\omega) & M_{12}(\omega) \\ M_{21}(\omega) & QS2(\omega) \end{bmatrix}\underset{\sim}{\mathbf{C}}^T(\alpha_S) \qquad (9)$$

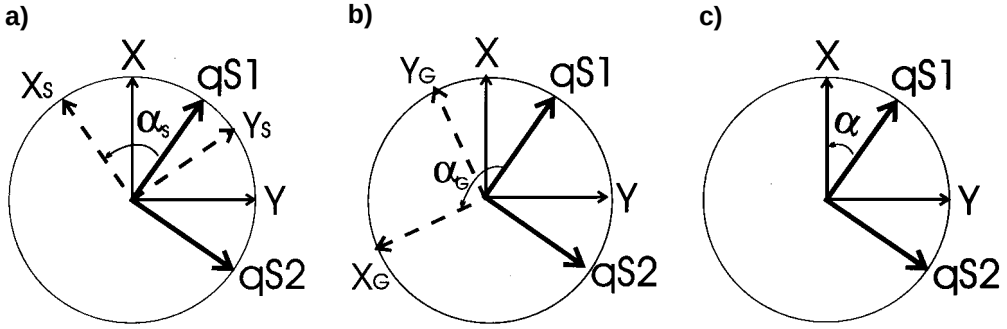

FIG. 2. The four-component coordinate system: (a) sources misoriented at α_S direction from the $qS1$ direction; (b) geophones misoriented at α_G direction; (c) both source and geophone aligned along the α direction.

where,

$$\underset{\sim}{\mathbf{C}}(\alpha) = \begin{bmatrix} \cos\alpha & \sin\alpha \\ -\sin\alpha & \cos\alpha \end{bmatrix}, \tag{10}$$

is a standard rotation matrix. The diagonal elements $QS1(\omega)$ and $QS2(\omega)$ are the medium responses for each split shear wave, $M_{12}(\omega)$ is the medium response for the converted wave from $qS1$ to $qS2$, and $M_{21}(\omega)$ is the converted wave response from $qS2$ to $qS1$. To calculate the asymmetry indices, we transform equation (9) back to the time domain and introduce $qS1(t), qS2(t), m_{12}(t)$, and $m_{21}(t)$ as the corresponding shear-wave responses in the time domain. We may write

$$\underset{\sim}{\mathbf{d}}(t) = \underset{\sim}{\mathbf{C}}(\alpha_G)\begin{bmatrix} qS1(t) & m_{12}(t) \\ m_{21}(t) & qS2(t) \end{bmatrix}\underset{\sim}{\mathbf{C}}^T(\alpha_S). \tag{11}$$

Substituting equation (11) into equation (5) gives

$$\begin{bmatrix} \zeta(t) \\ \chi(t) \end{bmatrix} = \underset{\sim}{\mathbf{C}}(\alpha_G - \alpha_S)\begin{bmatrix} a(t) \\ b(t) \end{bmatrix}, \tag{12}$$

where,

$$\begin{aligned} a(t) &= qS1(t) + qS2(t); \\ b(t) &= m_{12}(t) - m_{21}(t). \end{aligned} \tag{13}$$

Equation (12) shows that the linearity of motion (ζ, χ) is determined by the linearity of motion (a, b). Letting $\Delta\theta_{ab}$ be the angle between the major axis of motion (a, b) and axis $a(t)$, and letting γ_{ab} be the nonlinearity of motion (a, b), as shown in Figure 3, we then can write the asymmetry indices $\gamma(\tau)$ and $\Delta\theta(\tau)$ for data matrix $\underset{\sim}{\mathbf{d}}(t)$ as

$$\gamma(\tau) = \gamma_{ab}(\tau); \qquad \Delta\theta(\tau) = \alpha_S - \alpha_G + \Delta\theta_{ab}(\tau). \tag{14}$$

Although mode conversions often occur during wave propagation, for a given raypath the amplitude difference between the conversions from one mode to another and vice versa is likely small in most realistic cases compared with the unconverted shear-wave modes. In other words, $b(t)$ is very small compared with $a(t)$, hence $\gamma_{ab}(\tau)$ and $\Delta\theta_{ab}(\tau)$ will be small, as shown in Figure 3a. This implies that $\gamma(\tau)$ will be small in most realistic cases, and $\Delta\theta(\tau)$ will mainly measure the source-geophone misorientation. It also suggests that $\gamma(\tau)$ may serve as a quality factor for the data matrix. In an extreme condition where $b(t)$ is comparable with $a(t)$, $\gamma(\tau)$ will be significant, and $\Delta\theta(\tau)$ will contain an element of the source-geophone misorientation. However, if the phase difference between $a(t)$ and $b(t)$ is close to 90°, $\Delta\theta(\tau)$ will still mainly measure source-geophone misorientation (Figure 3b). Thus, we can conclude that in most cases the source-geophone misorientation can be determined from the index $\Delta\theta(\tau)$; the medium asymmetry can be determined from the index $\gamma(\tau)$.

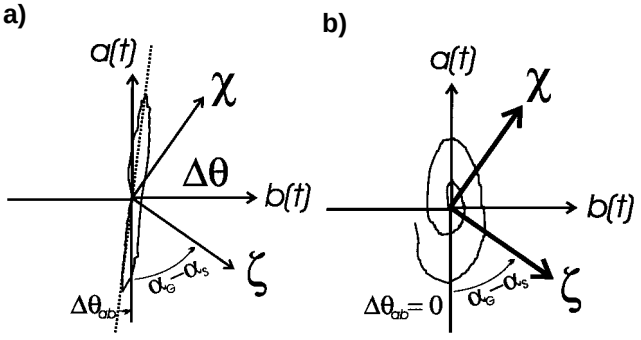

FIG. 3. The relationship between motion (ζ, χ) and motion $(a(t), b(t))$: (a) a small $b(t)$; (b) $a(t)$ and $b(t)$ with 90° phase difference.

Asymmetry caused by a polarization change at an interface

Consider a planar interface separating two anisotropic media, for which the $qS1$ polarizations of the downgoing waves are different (Figure 4), and there is no source or geophone misorientation. $\underset{\sim}{\mathbf{D}}(\omega)$ may be written, after correcting for the source signature and geophone response (MacBeth and Yardley, 1992) as

$$\underset{\sim}{\mathbf{D}}(\omega) = \underset{\sim}{\mathbf{C}}(\alpha)\underset{\sim}{\mathbf{\Lambda}}_U(\omega)\underset{\sim}{\mathbf{R}}\underset{\sim}{\mathbf{\Lambda}}_D(\omega)\underset{\sim}{\mathbf{C}}^T(\alpha) \tag{15}$$

where $\underset{\sim}{\mathbf{\Lambda}}_U(\omega)$ and $\underset{\sim}{\mathbf{\Lambda}}_D(\omega)$ are the diagonal phase-shift propagators for the up- and down-going shear waves, and $\underset{\sim}{\mathbf{R}}$ is the frequency-independent tensor reflectivity. Assuming negligible lateral variation, such that the reciprocity relation $\underset{\sim}{\mathbf{\Lambda}}_U(\omega) = \underset{\sim}{\mathbf{\Lambda}}_D^T(\omega) = \underset{\sim}{\mathbf{\Lambda}}_D(\omega)$ is fulfilled, then any data matrix asymmetry arises from the reflectivity matrix. The plane wave reflectivity matrix is

$$\begin{aligned} \underset{\sim}{\mathbf{R}} &= \begin{bmatrix} r_{11} & r_{21} \\ r_{12} & r_{22} \end{bmatrix} \\ &= \left(\underset{\sim}{\mathbf{X}}_1^{-1}\underset{\sim}{\mathbf{X}}_2 - \underset{\sim}{\mathbf{Y}}_1^{-1}\underset{\sim}{\mathbf{Y}}_2\right)\left(\underset{\sim}{\mathbf{X}}_1^{-1}\underset{\sim}{\mathbf{X}}_2 + \underset{\sim}{\mathbf{Y}}_1^{-1}\underset{\sim}{\mathbf{Y}}_2\right)^{-1}; \end{aligned} \tag{16}$$

where r_{ij} $(i, j = 1, 2)$ is the reflection coefficient from the ith mode (incident wave) to the jth mode. $\underset{\sim}{\mathbf{X}}_i$ and $\underset{\sim}{\mathbf{Y}}_i$ $(i = 1, 2)$ are frequency independent impedance matrices for the upper and lower media (Schoenberg and Protazio, 1992). For normally incident shear waves on an interface between media with orthorhombic symmetry or higher, we have (Appendix A)

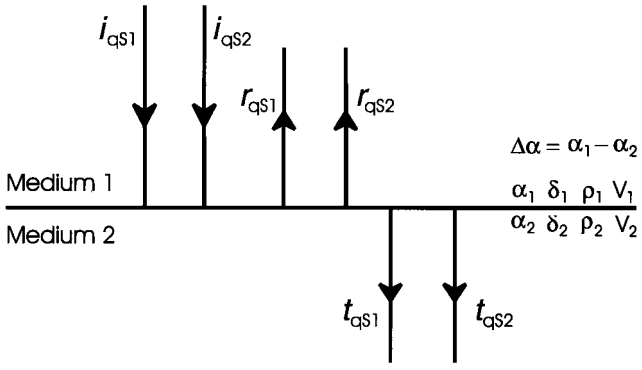

FIG. 4. Plane shear-wave reflection and transmission at a single anisotropic/anisotropic interface for near-vertical propagation. In the figure, i_{qS1} and i_{qS2} are the incident $qS1$ and $qS2$ waves, respectively; r_{qS1} and r_{qS2} are the reflected waves; and t_{qS1} and t_{qS2} are the transmitted waves. Also, α_i, δ_i, and v_i $(i = 1, 2)$ are, respectively, the polarization azimuth, degree of anisotropy, and the isotropic matrix velocity in the i-th layer; $\Delta\alpha = \alpha_1 - \alpha_2$, is the polarization change.

$$\underset{\sim}{\mathbf{X}}_1 = \begin{bmatrix} 0 & 1 \\ 1 & 0 \end{bmatrix}; \qquad \underset{\sim}{\mathbf{Y}}_1 = \begin{bmatrix} 0 & \rho_1(1-\delta_1)v_1 \\ \rho_1 v_1 & 0 \end{bmatrix};$$

$$\underset{\sim}{\mathbf{X}}_2 = \underset{\sim}{\mathbf{C}}(\Delta\alpha)\begin{bmatrix} 0 & 1 \\ 1 & 0 \end{bmatrix}, \tag{17}$$

$$\underset{\sim}{\mathbf{Y}}_2 = \underset{\sim}{\mathbf{C}}(\Delta\alpha)\begin{bmatrix} 0 & \rho_2(1-\delta_2)v_2 \\ \rho_2 v_2 & 0 \end{bmatrix};$$

where, as shown in Figure 4, δ_1, ρ_1, and v_1 are the degree of anisotropy, density, and matrix velocity in layer 1, respectively; δ_2, ρ_2, and v_2 are the corresponding parameters in layer 2; and $\Delta\alpha$ is the angular change in $qS1$ polarization from layer 1 to layer 2. If the $qS1$ polarization in the ith layer is $\alpha_i (i = 1, 2)$, then $\Delta\alpha = \alpha_2 - \alpha_1$.

Substituting equation (17) into equation (16) gives

$$\begin{aligned} \underset{\sim}{\mathbf{R}} = \begin{bmatrix} r_{11} & r_{21} \\ r_{12} & r_{22} \end{bmatrix} = \frac{-1}{I_0}\Bigg[& (\rho_2(1-\delta_2)v_2\rho_2 v_2 \\ & - \rho_1(1-\delta_1)v_1\rho_1 v_1)\underset{\sim}{\mathbf{I}} + \delta_2 \underset{\sim}{\mathbf{C}}(\Delta\alpha)\begin{bmatrix} -1 & 0 \\ 0 & 1 \end{bmatrix} \\ & \times \underset{\sim}{\mathbf{C}}^T(\Delta\alpha)(\rho_1 v_1\rho_2 v_2) + \delta_1\begin{bmatrix} 1 & 0 \\ 0 & -1 \end{bmatrix}(\rho_1 v_1\rho_2 v_2) \\ & + \delta_1\delta_2\begin{bmatrix} -\sin^2\Delta\alpha & 0 \\ -\sin 2\Delta\alpha & \sin^2\Delta\alpha \end{bmatrix}(\rho_1 v_1\rho_2 v_2)\Bigg]; \end{aligned} \tag{18}$$

$$\begin{aligned} I_0 = {} & [\rho_2(1-\delta_2)v_2 + \rho_1(1-\delta_1)v_1] \\ & \times (\rho_2 v_2 + \rho_1 v_1)\cos^2\Delta\alpha + [(\rho_2(1-\delta_2)v_2 + \rho_1 v_1] \\ & \times [\rho_2 v_2 + \rho_1(1-\delta_1)v_1]\sin^2\Delta\alpha. \end{aligned}$$

These equations agree with the alternative formulation of Li and Crampin (1993b). Although equation (18) appears complicated, only one term is asymmetric:

$$\delta_1\delta_2\begin{bmatrix} -\sin^2\Delta\alpha & 0 \\ -\sin 2\Delta\alpha & \sin^2\Delta\alpha \end{bmatrix}(\rho_1 v_1\rho_2 v_2). \tag{19}$$

This term is proportional to the product of δ_1 and δ_2, the anisotropies in the upper and lower layer. Thus this asymmetry caused by a polarization change is a second-order effect with respect to the degree of anisotropy, and is expected to be negligible. This is contrary to our expectations for VSP data, where such changes produce a significant effect on the data (MacBeth et al., 1994). The degree of this asymmetry may be judged visually by the numerical curves of Figure 5a, where the differences between r_{12} and r_{21} are very small. As demonstrated in equation (14), the asymmetry index $\gamma(\tau)$ will also be very small, and $\Delta\theta(\tau)$ will mainly measure the source-geophone misorientation. This result has two implications: (1) if there are polarization changes, we can still process the data to achieve an optimal separation of the split shear waves for a uniform overburden; (2) it may not be possible to detect true polarization changes directly from data matrix asymmetry unless there is a significant amount of anisotropy. However, relative changes of polarizations may still be detected, as the presence of mode conversion at the interface will change the polarization measurements. These aspects are illustrated by

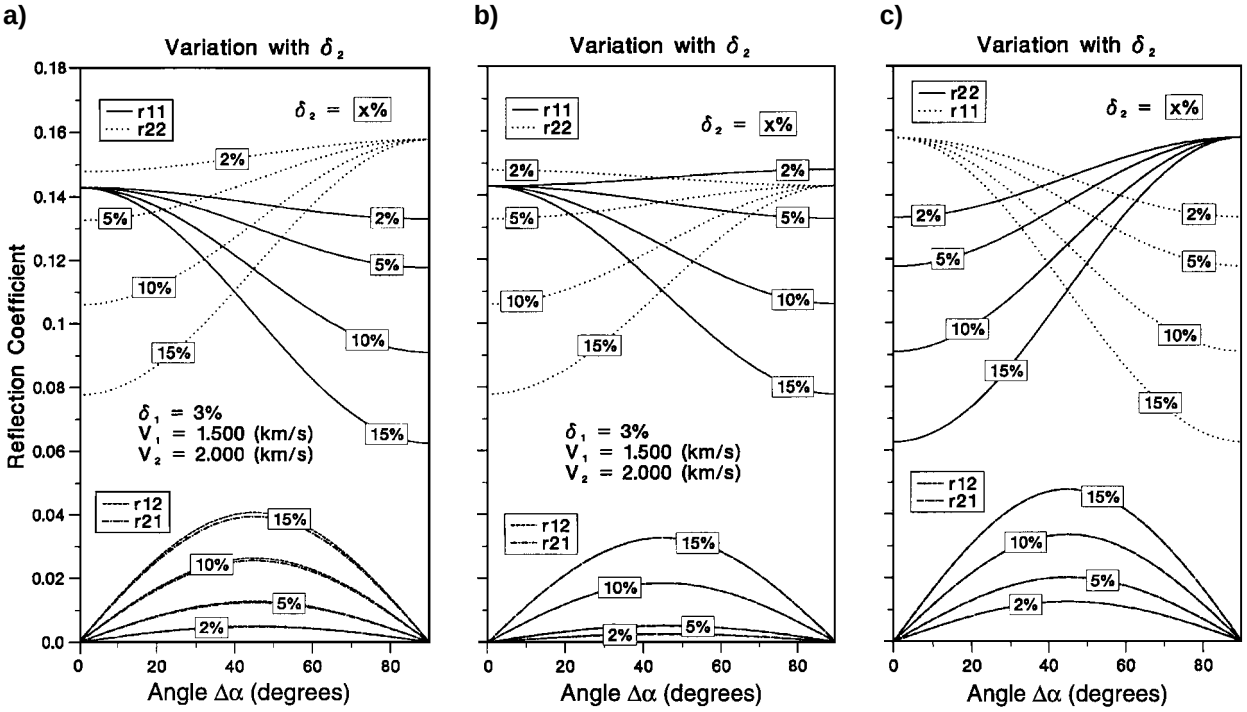

FIG. 5. (a) Reflection coefficients calculated from the exact analytic equation (18). The anisotropy in the upper layer is fixed at 3%, while the anisotropy in the lower layer varies from 2% to 15%. (b) Reflection coefficients calculated from the same model as in (a) but using the approximate equation (22) for small polarization changes. (c) Reflection coefficients calculated from the same model as in (a) but using the approximate equation (23) for large polarization changes.

constructing full-wave synthetic seismograms for the multilayered model of Figure 6, incorporating a polarization change in the reservoir zone in the middle of the third layer. Figure 7a shows the seismograms computed using the anisotropic reflectivity method (Taylor, 1990), and Figure 8 the corresponding asymmetry indices and polarization measurements, which are calculated for two locations A and B as shown in Figures 6 and 7a. Location A contains the zone of polarization changes (the solid line in Figure 8); location B contains no polarization change (the dots in Figure 8). The polarization measurements are calculated using the linear-transform technique (Li and Crampin, 1993a) for each event in Figure 7a. (The linear transforms are shown in equations (5) and (C-1) in Appendix C.) Note that both indices $\gamma(\tau)$ and $\Delta\theta(\tau)$ for locations A and B are zero (Figures 8a, b), indicating that the data matrix in Figure 7a are symmetric; however, the polarization measurements from location A show a change (Figure 8c) which corresponds to the zone of polarization changes.

Relative degrees of asymmetry

To sum up, the γ index measures the asymmetry in the medium response and is small for most realistic cases, while $\Delta\theta$ mainly measures the source-geophone misorientation. As a result, the reflection data matrix is more sensitive to asymmetry induced by the acquisition and other abnormally noisy conditions than from the medium properties such as reflectivity and anisotropy. The medium asymmetry caused by the change of polarization at an interface is proportional to the product of the degree of anisotropy in the layers, and is consequently a second-order effect. Although these conclusions are strictly for normal incidence, we would expect similar effects at small incidence angles.

Table 1. Isotropic parameters used in the model shown in Figure 6, where the anisotropy parameters are annotated.

	Density ρ (g/cm^3)	v_p (km/s)	v_S (km/s)
Layer 1	2.1	3.00	1.70
Layer 2	2.2	3.46	2.00
Layer 3a	2.2	4.33	2.50
Layer 3b	2.2	4.33	2.50
Layer 4	2.2	3.46	2.00
Layer 5	2.5	5.00	2.88

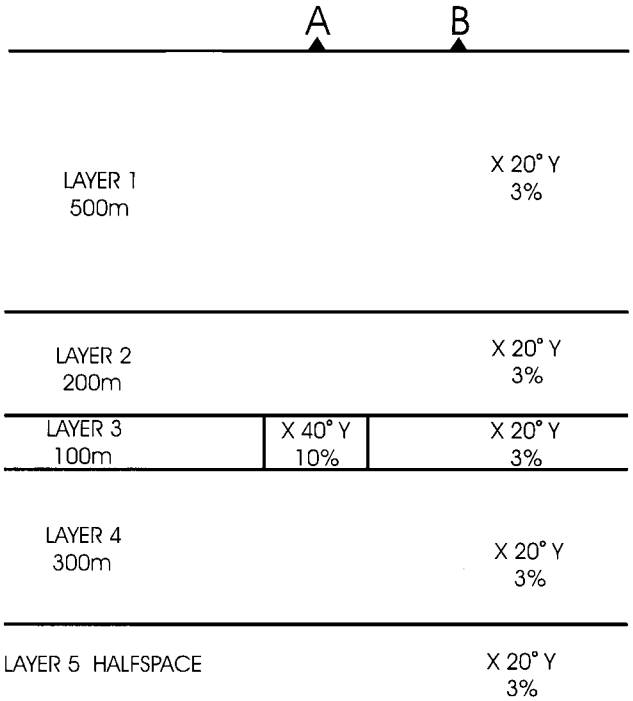

FIG. 6. Schematic earth model for south Texas containing a region with 10% shear-wave anisotropy in layer 3 simulating a fractured reservoir. The isotropic parameters are in Table 1, adapted from Yardley et al. (1991). A and B mark two locations for computing asymmetry indices.

INTERPRETING POLARIZATION CHANGES

The purpose of multicomponent data processing is to recover the principal time series and thus the principal reflectivity, as well as to retrieve the anisotropy information, particularly the $qS1$ polarization azimuth. Alford (1986), Thomsen (1988), and Li and Crampin (1993a) have presented methods for a uniform medium with azimuthal anisotropy. Here, we extend these methods for multicomponent seismic reflection data to accommodate polarization changes. We first introduce the concept of principal reflectivity, then present the simplified reflection coefficients for a vertically propagating shear-wave in media with polarization changes. Finally, a singular-value decomposition (SVD) technique is suggested as a practical solution to supersede these, and this is illustrated with both synthetic and real data examples.

Principal Reflectivity $\underset{\sim}{\mathbf{R}}_0^{\parallel}$ and $\underset{\sim}{\mathbf{R}}_0^{\perp}$

We refer to the reflectivity components for polarization changes of 0° or 90° as the principal reflectivities. Following Thomsen (1988), the first is denoted as $\mathbf{R}_0^{\parallel}$ and the second as $\mathbf{R}_0^{\perp}$. Substituting $\Delta\alpha = 0$ and $\Delta\alpha = \pi/2$, into equation (18) gives

$$\underset{\sim}{\mathbf{R}}_0^{\parallel} = \underset{\sim}{\mathbf{R}}(\Delta\alpha = 0) = \begin{bmatrix} R_1^{\parallel} & 0 \\ 0 & R_2^{\parallel} \end{bmatrix}$$

$$= \begin{bmatrix} \dfrac{(\rho_1 v_1 - \rho_2 v_2)}{(\rho_1 v_1 + \rho_2 v_2)} & 0 \\ 0 & \dfrac{\rho_1(1-\delta_1)v_1 - \rho_2(1-\delta_2)v_2}{\rho_1(1-\delta_1)v_1 + \rho_2(1-\delta_2)v_2} \end{bmatrix}; \tag{20}$$

$$\underset{\sim}{\mathbf{R}}_0^{\perp} = \underset{\sim}{\mathbf{R}}\left(\Delta\alpha = \frac{\pi}{2}\right) = \begin{bmatrix} R_1^{\perp} & 0 \\ 0 & R_2^{\perp} \end{bmatrix}$$

$$= \begin{bmatrix} \dfrac{(\rho_1 v_1 - \rho_2(1-\delta_2)v_2)}{(\rho_1 v_1 + \rho_2(1-\delta_2)v_2)} & 0 \\ 0 & \dfrac{\rho_1(1-\delta_1)v_1 - \rho_2 v_2}{\rho_1(1-\delta_1)v_1 + \rho_2 v_2} \end{bmatrix}. \tag{21}$$

For small $\Delta\alpha$, the reflectivity matrix of equation (18) can be approximated by

$$\underset{\sim}{\mathbf{R}} \approx \underset{\sim}{\mathbf{C}}(\Delta\alpha)\underset{\sim}{\mathbf{R}}_0^{\parallel}\underset{\sim}{\mathbf{C}}^T(\Delta\alpha) = \underset{\sim}{\mathbf{C}}(\Delta\alpha)\begin{bmatrix} R_1^{\parallel} & 0 \\ 0 & R_2^{\parallel} \end{bmatrix}\underset{\sim}{\mathbf{C}}^T(\Delta\alpha); \tag{22}$$

for $\Delta\alpha$ close to 90° ($|\Delta\alpha - \pi/2|$ is small), equation (18) can be approximated by

$$\underset{\sim}{\mathbf{R}} \approx \underset{\sim}{\mathbf{C}}(\Delta\alpha)\underset{\sim}{\mathbf{R}}_0^{\perp}\underset{\sim}{\mathbf{C}}^T(\Delta\alpha) = \underset{\sim}{\mathbf{C}}(\Delta\alpha)\begin{bmatrix} R_1^{\perp} & 0 \\ 0 & R_2^{\perp} \end{bmatrix}\underset{\sim}{\mathbf{C}}^T(\Delta\alpha). \tag{23}$$

Thus, as shown previously, the recorded data matrix is always likely to be essentially symmetric because the asymmetric part is considered to be small. To understand the accuracy and limits of these approximations, we calculate numerical curves, as shown in Figures 5b and 5c (for small and large changes, respectively), and compare them with the exact solutions in Figure 5a. We note that equation (22) is valid for $\Delta\alpha < 30°$

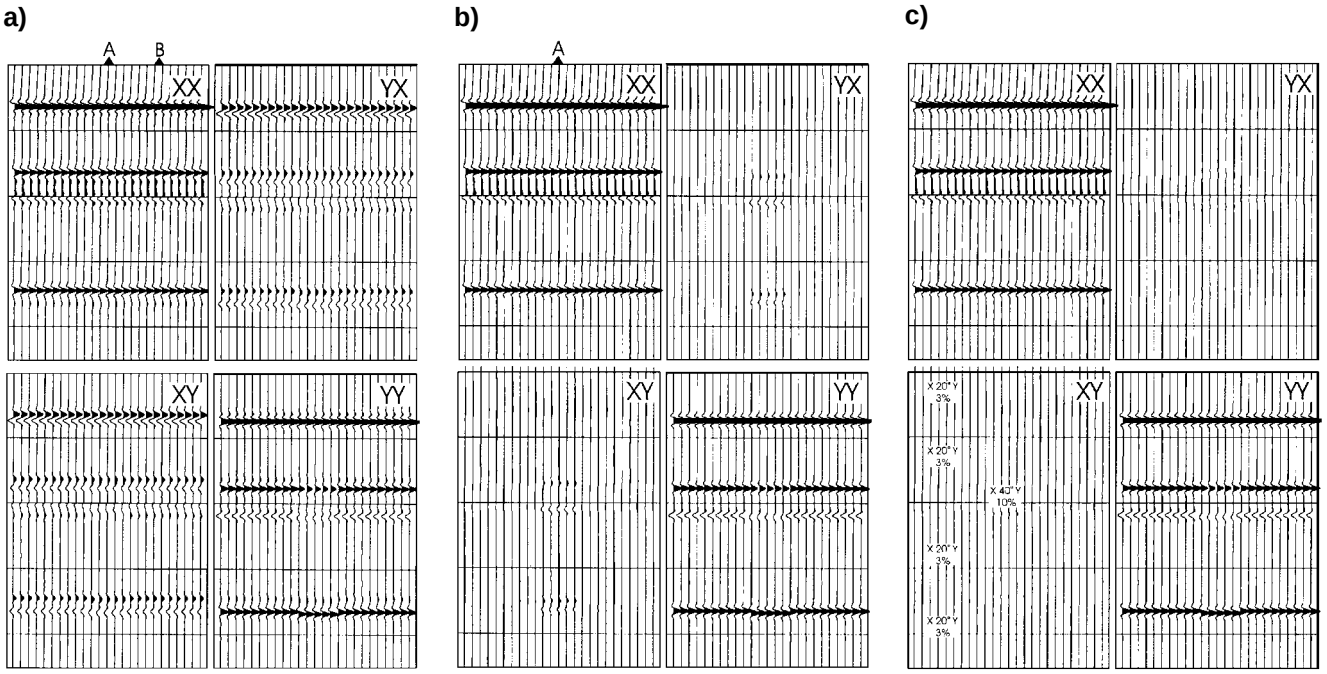

FIG. 7. (a) The synthetic data matrix for normally incident shear waves calculated using the anisotropic reflectivity method (Taylor, 1990) for the model in Figure 6. The strong coherent off-diagonal energy indicates shear-wave splitting. Traces at locations A and B are selected to compute asymmetry indices. (b) The data matrix after the first SVD, which corrects the overburden anisotropy and determines the background anisotropy parameters. The off-diagonal energy in (a) is largely minimized; there is only some residual energy in the off-diagonals, which is caused by the polarization change. Traces at location A are selected to compute asymmetry indices. (c) The principal data matrix, representing the principal reflectivity $\underset{\sim}{\mathbf{R}}_0^{\parallel}$, after the second SVD, which determines changes of anisotropy parameters. Note that the residual energy in the off-diagonals in (b) is almost fully eliminated.

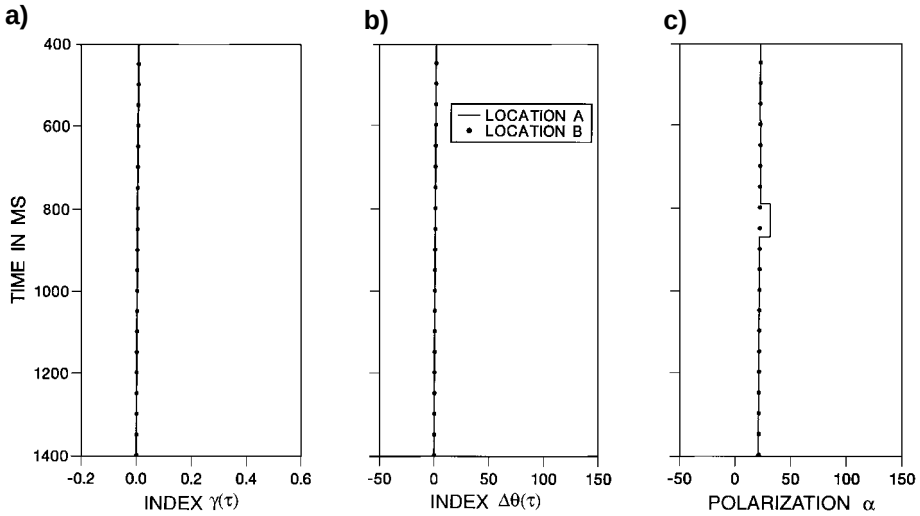

FIG. 8. Asymmetry indices and polarization measurements corresponding to the traces at locations A and B from the data matrix in Figure 7a: (a) γ index, (b) $\Delta\theta$ index, (c) polarization measurements. The solid line is calculated from traces at location A, and the dots from traces at location B. Some small relative changes in (c) highlight the zone of polarization change.

(Figure 5b), and that equation (23) is valid for $\Delta\alpha > 60^\circ$ (Figure 5c).

Detecting polarization changes

Assume a misorientation of source and receiver coordinate frames, but a uniform anisotropic overburden and a target zone with a change of the $qS1$ polarization of $\Delta\alpha$. Noting equations (15), (22), and (23), then replacing angle α with angles α_G and α_S we obtain for this reflector

$$\underset{\sim}{\mathbf{D}}(\omega) = \underset{\sim}{\mathbf{C}}(\alpha_G)\underset{\sim}{\Lambda}_U(\omega)\underset{\sim}{\mathbf{C}}(\Delta\alpha)\underset{\sim}{\mathbf{R}}_0\underset{\sim}{\mathbf{C}}^T(\Delta\alpha)\underset{\sim}{\Lambda}_D(\omega)\underset{\sim}{\mathbf{C}}^T(\alpha_S), \tag{24}$$

where $\underset{\sim}{\mathbf{R}}_0$ is a diagonal matrix containing either of the principal reflectivities $\underset{\sim}{\mathbf{R}}_0^{\parallel}$ or $\underset{\sim}{\mathbf{R}}_0^{\perp}$. Equation (24) shows that the predominant effect of the polarization change is to introduce extra rotation operators dependent upon $\Delta\alpha$. The upgoing diagonal propagator $\Lambda_U(\omega)$ and downgoing diagonal propagator $\Lambda_D(\omega)$ are equal:

$$\underset{\sim}{\Lambda}_U(\omega) = \underset{\sim}{\Lambda}_D(\omega) = \begin{bmatrix} 1 & 0 \\ 0 & e^{-i\omega\Delta t} \end{bmatrix}, \tag{25}$$

where Δt is the time delay between the $qS1$ and $qS2$ waves, and the common phase-shift operator $e^{-i\omega t}$ is omitted. It is now possible to solve equation (24) using a layer-stripping technique, as demonstrated in MacBeth et al. (1992), to determine the anisotropy parameters and the principal reflectivity. The layer-stripping procedure can be implemented using a series of SVDs, or a series of rotations if there is no source or geophone misorientation. The following procedure can be adopted in the data analysis:

1) Apply multicomponent amplitude corrections (Li, 1994) to compensate for the source signature and geophone response based on equation (3), and obtain $\underset{\sim}{\mathbf{M}}(\omega)$, and its time domain correspondent $\underset{\sim}{\mathbf{m}}(t)$.
2) Examine the asymmetry index $\Delta\theta(\tau)$ to determine the degree of acquisition error and $\gamma(\tau)$ to examine the quality of data and determine the degree of asymmetry in the medium response.
3) Given this asymmetry, apply an SVD to $\underset{\sim}{\mathbf{m}}(t)$ over the entire time window to find the average polarization angles α_G and α_S that minimize the off-diagonal elements of $\underset{\sim}{\mathbf{m}}(t)$ to obtain $\underset{\sim}{\mathbf{M}}_1(\omega) = \underset{\sim}{\mathbf{C}}^T(\alpha_G)\underset{\sim}{\mathbf{M}}(\omega)\underset{\sim}{\mathbf{C}}^T(\alpha_S)$, and its time domain correspondent $\underset{\sim}{\mathbf{m}}_1(t)$. This may be implemented using the linear-transform technique in Li and Crampin (1993a) or the formulas in Zeng and MacBeth (1993b). Alternatively, independent information from VSPs in the same area may also be used to tie to these values.
4) Estimate the average time delay Δt from the two diagonal elements in $\underset{\sim}{\mathbf{m}}_1(t)$ using the cross-correlation method or manual picking over the reflection events in the overburden, and calculate $\underset{\sim}{\mathbf{M}}_2(\omega) = \underset{\sim}{\Lambda}_U^{-1}(\omega)\underset{\sim}{\mathbf{M}}_1(\omega)\underset{\sim}{\Lambda}_D^{-1}(\omega)$, and $\underset{\sim}{\mathbf{m}}_2(t)$, which is equivalent to a phase shift in the frequency domain and time shift in the time domain.
5) Apply the SVD again to $\underset{\sim}{\mathbf{m}}_2(t)$ on a trace-by-trace basis to determine the changes of polarization angle $\Delta\alpha$ and the principal reflectivity $\underset{\sim}{\mathbf{R}}_0$.

Here, the synthetic data set in Figure 7a is used to illustrate the procedure, and some intermediate results are displayed. Figures 8a and 8b show the asymmetry indices, as discussed previously. Figures 7b and 7c show, respectively, the data matrix of $\underset{\sim}{\mathbf{m}}_1(t)$ after the third step and the principal reflectivity matrix $\underset{\sim}{\mathbf{R}}_0$ after the fifth step. Comparing Figures 7a and 7b shows that the off-diagonal elements in Figure 7a are minimized and the overburden anisotropy is corrected. The residual energy in Figure 7b indicates variations in medium properties. The residual energy in the off-diagonals in Figure 7b is also minimized after the second SVD, as shown in the principal reflectivity matrix in Figure 7c, and a clear amplitude dimming can be identified, corresponding to the reservoir zone. Figure 9 shows polarization changes $\Delta\alpha$ for the traces at location A after the fifth step; the absolute polarization change of 20° is recovered corresponding to the reservoir zone in Figure 6.

Real data application

Although the above layer-stripping sequence allows recovery of absolute polarization changes, successful application of the sequence requires almost noise-free high-quality data. A similar layer-stripping technique has been successfully applied to multicomponent VSPs (Winterstein and Meadows, 1991), where high quality data are common. However, most real shear-wave reflection data may not satisfy this condition.

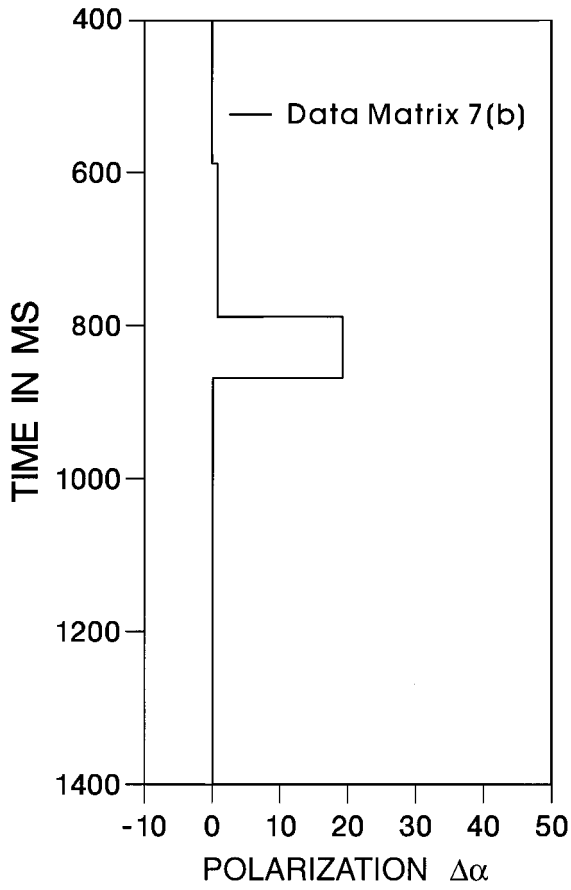

FIG. 9. The absolute polarization changes calculated from traces at location A in the data matrix in Figure 7b using a window for each event determined by the layer-stripping sequence based on equation (24). A polarization change of 20° is determined for the reservoir zone.

Besides, it is also very difficult to window the reflection data accurately, and the boundaries of polarization changes may not coincide with the lithological (impedance) boundaries (Winterstein and Meadows, 1991), which are other essential requirements for achieving an effective layer stripping for surface-seismic reflection data (MacBeth et al., 1992). Considering the fact that abnormal zones of relative polarization changes may be more significant than absolute values, we thus search for an alternative approach to the above layer-stripping sequence for application to real shear-wave surface-seismic reflection data, which aims only to recover the relative changes. Our approach is to further approximate equation (24), so that it can be solved effectively and robustly, and information obtained can be interpreted meaningfully.

Noting that $\Delta\alpha$ is close to 0° or 90°, we may further approximate equation (24) as (see Appendix B)

$$\underset{\sim}{\mathbf{D}}(\omega) \approx \underset{\sim}{\mathbf{C}}(\alpha_G + \Delta\alpha)\underset{\sim}{\mathbf{R}}_p(\omega)\underset{\sim}{\mathbf{C}}^T(\alpha_S + \Delta\alpha). \qquad (26)$$

The diagonal phase-shift operators $\underset{\sim}{\Lambda}_U(\omega)$ and $\underset{\sim}{\Lambda}_D(\omega)$ in equation (24) have now been absorbed into the term $\underset{\sim}{\mathbf{R}}_p(\omega)$,

$$\underset{\sim}{\mathbf{R}}_p(\omega) = \begin{bmatrix} QS_1(\omega) & O(\omega) \\ O(\omega) & QS_2(\omega) \end{bmatrix}, \qquad (27)$$

where $QS_1(\omega)$ and $QS_2(\omega)$ are the principal modes associated with the principal reflectivity $\underset{\sim}{\mathbf{R}}_0$; $O(\omega)$ is a residual term representing the interferences between the principal and converted modes, and is very small compared with the principal modes in $\underset{\sim}{\mathbf{R}}_p(\omega)$, as shown in equation (B-8) in Appendix B. Thus the γ index obtained from equation (26) will be small in most realistic cases and $\Delta\theta$ again mainly measures source-geophone misalignment, as discussed previously in equation (14); the γ index may serve as a good quality factor for checking the reflection data matrix, and any abnormal γ values may indicate pathological conditions. The asymmetry has to be corrected before relative polarization changes can be interpreted. After correcting the source and geophone misorientation and letting $\alpha_G = \alpha_S = \alpha$, equation (26) can be written as

$$\underset{\sim}{\mathbf{D}}(\omega) \approx \underset{\sim}{\mathbf{C}}(\alpha + \Delta\alpha)\underset{\sim}{\mathbf{R}}_p(\omega)\underset{\sim}{\mathbf{C}}^T(\alpha + \Delta\alpha). \qquad (28)$$

Because the off-diagonals in $\underset{\sim}{\mathbf{R}}_p(\omega)$ are very small compared with the diagonals, the polarization angles obtained from $\underset{\sim}{\mathbf{D}}(\omega)$ by using the linear transform technique (an SVD procedure) in $\underset{\sim}{\mathbf{D}}(\omega)$ will be close to the angle $\alpha + \Delta\alpha$, as discussed in Appendix C. Thus it is now possible to establish a practical processing sequence to interpret the relative polarization changes from real data. The following alternative procedure to the layer-stripping sequence may be adopted in real data analysis:

1) Apply multicomponent amplitude corrections (Li, 1994) to compensate for the source signature and geophone response based on equation (3). Examine the asymmetry indicators to determine the degree of acquisition error, if any. Apply an SVD based on equation (24) to determine and correct the source-geophone misorientation. These steps are the same as the first three steps in the layer-stripping sequence.
2) Apply the SVD again (or a similarity transform) using a sliding time window τ by the linear-transform technique (Li and Crampin, 1993a, Appendix C) to the data matrix after compensating for the source signature, geophone response, and misorientation in step (1) above. Thus, we can obtain a window-based instantaneous polarization angle $\alpha(\tau)$, which approximately equals the sum of the overburden average polarization angles and the angle of polarization change based on equation (28), and an instantaneous reflectivity matrix $\underset{\sim}{\mathbf{R}}_p$, of which the diagonal elements represent the principal reflectivity.
3) Display $\alpha(\tau)$ in color-coded sections based on the complex component analysis in Li and Crampin (1991). Thus zones of polarization changes will be identified by different polarization colors, and the background average polarization may then be identified by a majority polarization color.

In the above procedure, we use a window-based linear-transform technique (an instantaneous SVD) to replace the layer-stripping procedure, and we use color displays to interpret the background average polarization and identify zones of relative polarization changes, based on the approximate equations (26) and (28). Both steps can be effectively implemented, and are more robust and computing-efficient than the layer-stripping sequence.

Here, we use a multicomponent survey in south Texas to illustrate the procedure. This data are also used by Li et al. (1993) and Li (1994), where more details of the data can be found, to demonstrate shear-wave splitting and amplitude anomalies. Figure 10 shows a shot-record matrix of the data with amplitude corrections applied to remove the source signature and geophone response. We first examine the degree of asymmetry in the data matrix and correct for the source or geophone misorientation. To understand the variations of asymmetry indices in real data, we also deliberately rotated the receivers 20° for the common shot records shown in Figure 10. The indices for the original and the rotated data matrix are displayed as time functions in Figure 11. The dotted lines correspond to the original data matrix in Figure 10, the solid lines correspond to the rotated data matrix. They show that there are no overall changes in $\gamma(\tau)$ before and after rotating the receivers (Figure 11a), with $\Delta\theta(\tau)$ displaying a static 20° shift (Figure 11b). This effectively demonstrates that the γ index measures the medium asymmetry and is independent of rotation, and the $\Delta\theta$ index measures the source-geophone misorientation. Note that the γ index is generally small except for some changes in the near-surface, and the original angular index $\Delta\theta$ is close to zero, suggesting that the data matrix in Figure 10 is generally symmetric, and that the source and geophone are well aligned. Thus we can now proceed to processing the data and obtain a stacked data matrix, then apply steps 2 and 3 directly to the stacked data matrix. The results $\alpha(\tau)$ are displayed in Figure 12 in gray scale. Here the target is the Austin Chalk. Zones of polarization changes along the Austin Chalk can be identified which may be correlated with the fracture swarms in the Chalk (Li, 1994; Li and MacBeth, 1995). The change of polarization may be more indicative of large open fractures or pore pressure changes than interval time delay measurements and is easy to obtain reliably.

CONCLUSIONS

There are two main sources of asymmetry in the recorded data matrix from multicomponent surface seismics: that due

to acquisition conditions and that arising from subsurface polarization changes. The asymmetry caused by polarization changes is proportional to the product of the amount of anisotropy in the layers above and below a reflector, being quite small for most realistic cases. Two asymmetry indices, γ and $\Delta\theta$, may be used to obtain a quantitative measure of the asymmetry in the reflection data matrix, based upon a simple transformation of the multicomponent matrix. The γ index measures the medium asymmetry and is small in most realistic cases, while the $\Delta\theta$ index mainly measures acquisition asymmetry.

We have shown that although the reflection data matrix from surface surveys is often less informative than the transmission data matrix derived from VSPs, it can still be used for recovering some relative changes of polarization. For this purpose, we have derived simple approximate equations of the reflectivity matrix for vertically propagating plane shear waves. The reflection data matrix can then be approximated by rotating the principal reflectivity with the angle of polarization changes. Changes in polarization azimuth and the principal shear-wave reflectivity may then be recovered by using an instantaneous SVD (singular value decomposition) procedure.

ACKNOWLEDGMENTS

We thank Amoco Production Company for permission to use the multicomponent data. We thank David Booth and Enru Liu for comment on the manuscript, and Jim Brown for a thorough and helpful review of the paper. This work was supported by the Edinburgh Anisotropy Project and the Natural Environment Research Council, and is published with the approval of the Director of the British Geological Survey (NERC) and EAP sponsors.

REFERENCES

Alford, R. M., 1986, Shear data in the presence of azimuthal anisotropy: 56th Ann. Internat. Mtg., Soc. Expl. Geophys., Expanded Abstracts, 476–479.

Bruno, M. S., and Winterstein, D. F., 1994, Some influences of stratigraphy and structure on reservoir stress orientation: Geophysics, **59**, 954–962.

Hudson, J. A., 1981, Wave speed and attenuation of elastic waves in a material containing cracks: Geophys. J. Roy. Astr. Soc., **64**, 133–150.

Kanasewich, E. R., 1981, Time sequence analysis in Geophysics: Univ. of Alberta Press.

Lefeuvre, F., Nicoletis, L., Ansel, V., and Cliet, C., 1992, Detection and measure of the shear-wave birefringence from vertical seismic data: theory and applications: Geophysics, **57**, 1463–1481.

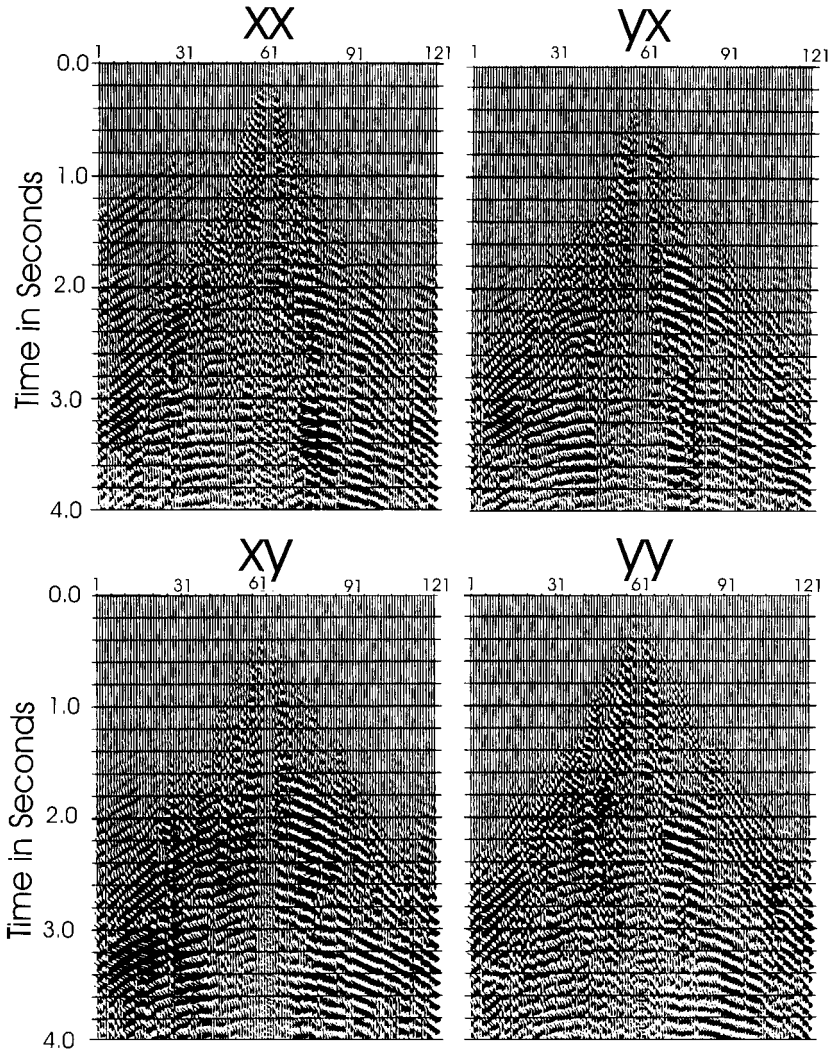

FIG. 10. A shot-record matrix selected from a multicomponent surface line in south Texas. Here, it is used to illustrate the relative polarization changes in field data.

Lewis, C., Davis, T. L., and Vuillermoz, C., 1991, Three-dimensional multicomponent imaging of reservoir heterogeneity, Silo Field, Wyoming: Geophysics, **56**, 2048–2056.
Li, X.-Y., 1994, Amplitude corrections for multicomponent surface seismic data: 64th Ann. Internat. Mtg., Soc. Expl. Geophys., Expanded Abstracts, 1505–1508.
Li, X.-Y., and Crampin, S., 1991, Complex component analysis of shear-wave splitting: theory: Geophys. J. Internat., **107**, 597–604.
———1993a, Linear-transform techniques for processing shear-wave anisotropy in four-component seismic data: Geophysics, **58**, 240–256.
———1993b, Variation of reflection coefficients with crack strike and crack density in anisotropic media: Geophys. Prosp., **41**, 859–882.
Li, X.-Y., and MacBeth, C., 1995, Interpreting data matrix asymmetry and polarization changes with depth in multicomponent reflection surveys: 65th Ann. Internat. Mtg., Soc. Expl. Geophys., Expanded Abstracts, 719–722.
Li, X.-Y., Mueller, M. C., and Crampin, S., 1993, Case studies of shear-wave splitting in reflection surveys in south Texas: Can. J. Expl. Geophys., **29**, 189–215.
MacBeth, C., Li, X.-Y., and Mueller, C. M., 1992, Detecting lateral variability in fracture parameters from surface seismic data: 62th Ann. Internat. Mtg., Soc. Expl. Geophys., Expanded Abstracts, 816–819.

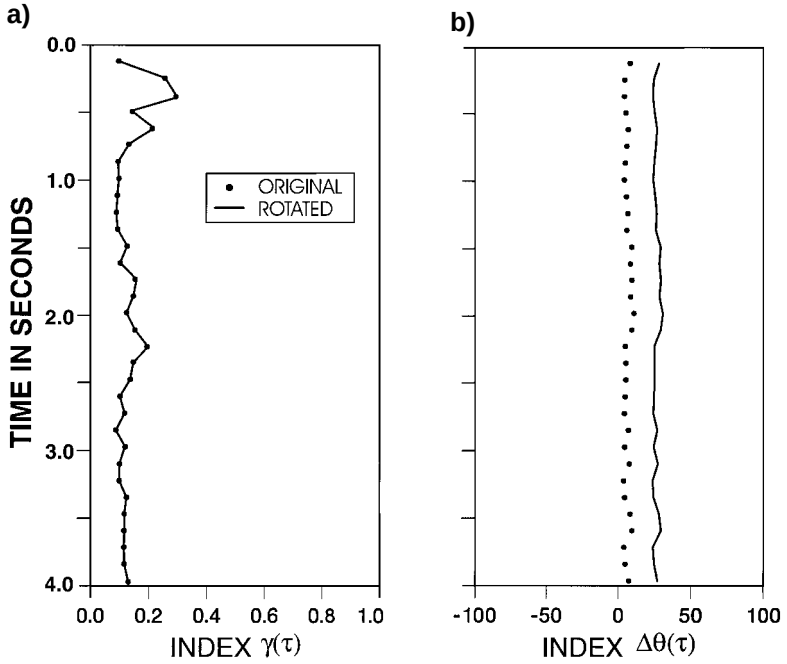

FIG. 11. Asymmetry indices (a) $\gamma(\tau)$ and (b) $\Delta\theta(\tau)$ calculated from the shot-record matrix in Figure 10. The dots are values calculated from the original data; the solid lines are values from the rotated data matrix whose geophone directions are deliberately rotated by 20°.

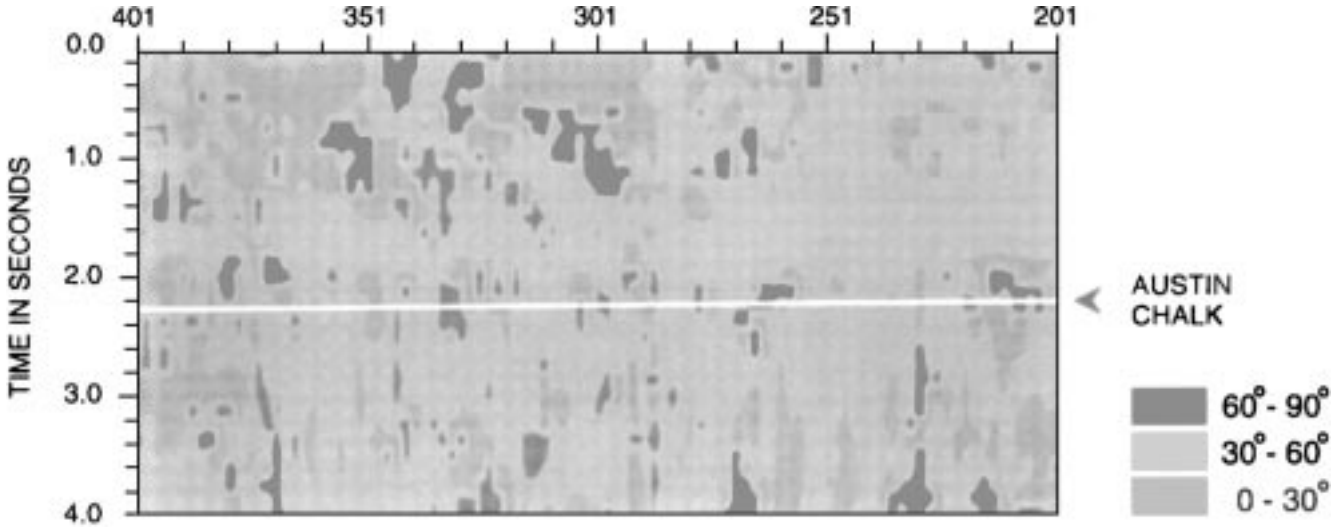

FIG. 12. Contour map of polarization section showing the polarization changes calculated from the multicomponent seismic line in Figure 10 by applying the window-based linear-transform technique to equation (28). The section is dominated by the background light gray color, indicating an average background polarization azimuth of 40°. There are significant polarization changes in the near-surface and along the Austin Chalk, marked by the zones of dark gray color. The polarization anomalies along the Austin Chalk trend may be correlated with the fracture swarms within the Chalk (Li, 1994; Li and MacBeth, 1995).

MacBeth, C., and Yardley, G., 1992, Optimal estimation of crack-strike: Geophys. Prosp., **40**, 849–872.
MacBeth, C., Zeng, X., Yardley, G., and Crampin, S., 1994, Interpreting data matrix asymmetry in near-offset shear-wave VSP data: Geophysics, **59**, 176–191.
Schoenberg, M., and Protazio, J., 1992, 'Zoeppritz' rationalized and generalized to anisotropy: J. Seis. Expl., **1**, 125–144.
Squires, S. G., Kim, C. D., and Kim, D. Y., 1989, Interpretation of total wavefield data over Lost Hills Field, Kern County, California: Geophysics, **54**, 1420–1429.
Taylor, D. B., 1990, Aniseis manual: Version 4.5: Applied Geophysical Software.
Thomsen, L. A., 1988, Reflection seismology over azimuthally anisotropic media: Geophysics, **53**, 304–313.
Warpinski, N. R., and Teufel, L. W., 1991, In situ stress measurements of Rainier Mesa, Nevada Test Site—influence of topography and lithology on the stress state in Tuff: Internat. J. Rock Mech., Min. Sci. & Geomechanical Abstracts, **28**, 143–161.
Winterstein, D. F., and Meadows, M. A., 1991, Shear-wave polarization and subsurface stress directions at Lost Hills field: Geophysics, **56**, 1331–1348.
Yardley, G. S., Graham, G., and Crampin, S., 1991, Viability of shear-wave amplitude versus offset studies in anisotropic media: Geophys. J. Internat., **107**, 493–503.
Zeng, X., and MacBeth, C., 1993a, Multicomponent deconvolution algorithm for VSP data for shear-wave splitting. Joint Mtg. Soc. Expl. Geophys. & Chin. Petr. Soc., Expanded Abstracts, 479–482.
———1993b, Algebraic processing techniques for estimating shear-wave splitting in near-offset VSP data: Theory: Geophys. Prosp., **41**, 1033–1066.

APPENDIX A

THE DERIVATION OF THE REFLECTIVITY MATRIX

Here, we rederive the equations of Li and Crampin (1993b) using the matrix notation suggested by Schoenberg and Protazio (1992). Consider two anisotropic half spaces with orthorhombic or higher class of symmetry separated by the horizontal $x_1 - x_2$-plane, with the x_3-axis positive downward. Thus we have the following stress-strain relation:

$$\begin{bmatrix}\sigma_{11}\\ \sigma_{22}\\ \sigma_{33}\\ \sigma_{23}\\ \sigma_{31}\\ \sigma_{12}\end{bmatrix} = \begin{bmatrix} c_{11} & c_{12} & c_{13} & 0 & 0 & 0\\ c_{12} & c_{22} & c_{23} & 0 & 0 & 0\\ c_{13} & c_{23} & c_{33} & 0 & 0 & 0\\ 0 & 0 & 0 & c_{44} & 0 & 0\\ 0 & 0 & 0 & 0 & c_{55} & 0\\ 0 & 0 & 0 & 0 & 0 & c_{66}\end{bmatrix}\begin{bmatrix}\epsilon_{11}\\ \epsilon_{22}\\ \epsilon_{33}\\ \epsilon_{23}\\ \epsilon_{31}\\ \epsilon_{12}\end{bmatrix}, \tag{A-1}$$

where σ_{ij} and ϵ_{ij} $(i, j = 1, 2, 3)$ are stress and strain tensors, respectively, and c_{ij} $(i, j = 1, 2, \ldots, 6)$ a tensor of elastic constants. Using u_i to represent the displacement components along axis x_i $(i = 1, 2, 3)$ leads to

$$\begin{aligned}\epsilon_{ij} &= \frac{\partial u_i}{\partial x_j} + \frac{\partial u_j}{\partial x_i}, \quad \text{if} \quad i \neq j;\\ \epsilon_{ij} &= \frac{\partial u_i}{\partial x_j}, \quad \text{if} \quad i = j.\end{aligned} \tag{A-2}$$

Assume vertical propagation of two quasi–shear waves $qS1$ and $qS2$ uncoupled from the quasi-compressional waves polarized along the ray. Thus, the plane stress and strain tensors and the displacement vector have components only on a constant-x_3 plane; they are σ_{31} and σ_{32}, ϵ_{31} and ϵ_{32}, and u_1 and u_2, respectively. Equations (A-1) and (A-2) can be reduced and combined as

$$\begin{aligned}\begin{bmatrix}\sigma_{32}\\ \sigma_{31}\end{bmatrix} &= \begin{bmatrix} c_{44} & 0\\ 0 & c_{55}\end{bmatrix}\frac{\partial}{\partial x_3}\begin{bmatrix}u_2\\ u_1\end{bmatrix}\\ &= \begin{bmatrix}\rho v_{qS1}^2 & 0\\ 0 & \rho v_{qS2}^2\end{bmatrix}\frac{\partial}{\partial x_3}\begin{bmatrix}u_2\\ u_1\end{bmatrix},\end{aligned} \tag{A-3}$$

where v_{qS1} and v_{qS2} are the vertical velocities of $qS1$ and $qS2$ waves, respectively. We assume, without loss of generality, that the polarization direction of $qS1$ is along the x_2-axis.

The displacement field in the incident medium (medium 1) caused by incident and reflected $qS1$ and $qS2$ for $x_3 < 0$ can be written as

$$\begin{aligned}\begin{bmatrix}u_1\\ u_2\end{bmatrix} &= i_{qS1}\begin{bmatrix}0\\ 1\end{bmatrix}e^{i\omega x_3/v_{qS1}} + r_{qS1}\begin{bmatrix}0\\ 1\end{bmatrix}e^{-i\omega x_3/v_{qS1}}\\ &\quad + i_{qS2}\begin{bmatrix}1\\ 0\end{bmatrix}e^{i\omega x_3/v_{qS2}} + r_{qS2}\begin{bmatrix}1\\ 0\end{bmatrix}e^{-i\omega x_3/v_{qS2}}\end{aligned} \tag{A-4}$$

where i_{qS1} and i_{qS2} are incident amplitudes of $qS1$ and $qS2$ waves, respectively; r_{qS1} and r_{qS2} are the reflected amplitudes (Figure 4); a common phase factor $e^{i\omega t}$ is omitted. Introducing

$$\begin{aligned}\mathbf{i} &= \begin{bmatrix}i_{qS1}\\ i_{qS2}\end{bmatrix}; \qquad \mathbf{r} = \begin{bmatrix}r_{qS1}\\ r_{qS2}\end{bmatrix};\\ \underset{\sim}{\Lambda}(x_3) &= \begin{bmatrix}e^{i\omega x_3/v_{qS1}} & 0\\ 0 & e^{i\omega x_3/v_{qS2}}\end{bmatrix},\end{aligned} \tag{A-5}$$

and performing some manipulations of equation (A-4) gives

$$\begin{bmatrix}u_1\\ u_2\end{bmatrix} = \begin{bmatrix}0 & 1\\ 1 & 0\end{bmatrix}\left[\underset{\sim}{\Lambda}(x_3)\mathbf{i} + \underset{\sim}{\Lambda}^{-1}(x_3)\mathbf{r}\right]. \tag{A-6}$$

Substituting equation (A-6) into equation (A-3) yields

$$\begin{bmatrix}\sigma_{31}\\ \sigma_{32}\end{bmatrix} = (i\omega)\begin{bmatrix}0 & \rho_1 v_{qS2}\\ \rho_1 v_{qS1} & 0\end{bmatrix}\left[\underset{\sim}{\Lambda}(x_3)\mathbf{i} - \underset{\sim}{\Lambda}^{-1}(x_3)\mathbf{r}\right]. \tag{A-7}$$

The displacement and stress components in the medium of transmission (medium 2) can be similarly derived with two modifications. Firstly, we assume there is no upgoing wave but only downgoing transmitted waves t_{qS1} and t_{qS2} in medium 2; and analogous with equations (A-6) and (A-7), $\mathbf{i}$ should be replaced by $\mathbf{t} = (t_{qS1}, t_{qS2})^T$ and $\mathbf{r}$ is set to $\mathbf{0}$. Secondly, there is a polarization change of $\Delta\alpha$ from medium 1 to medium 2, which results in a coordinate rotation of $\Delta\alpha$ between the local coordinate system of medium 2 and the global coordinate system medium 1. Thus, we have

$$\begin{bmatrix}u_1\\ u_2\end{bmatrix} = \underset{\sim}{\mathbf{C}}(\Delta\alpha)\begin{bmatrix}0 & 1\\ 1 & 0\end{bmatrix}\underset{\sim}{\Lambda}(x_3)\mathbf{t}, \tag{A-8}$$

and

$$\begin{bmatrix}\sigma_{31}\\ \sigma_{32}\end{bmatrix} = (i\omega)\underset{\sim}{\mathbf{C}}(\Delta\alpha)\begin{bmatrix}0 & \rho_2 v'_{qS2}\\ \rho_2 v'_{qS1} & 0\end{bmatrix}\underset{\sim}{\Lambda}(x_3)\mathbf{t}, \quad \text{(A-9)}$$

where $\underset{\sim}{\mathbf{C}}(\Delta\alpha)$ is the rotation matrix defined by equation (10), which transforms measurements of medium 2 in the local natural coordinate system to the global coordinate system; ρ_2 is the density, and v'_{qS1} and v'_{qS2} are the vertical velocities of $qS1$ and $qS2$ in medium 2.

At the interface $x_3 = 0$, the displacement and stress components are continuous and $\underset{\sim}{\Lambda}(x_3 = 0) = \underset{\sim}{\mathbf{I}}$, the identity matrix, yielding

$$\begin{bmatrix}0 & 1\\ 1 & 0\end{bmatrix}(\mathbf{i}+\mathbf{r}) = \underset{\sim}{\mathbf{C}}(\Delta\alpha)\begin{bmatrix}0 & 1\\ 1 & 0\end{bmatrix}\mathbf{t}, \quad \text{(A-10)}$$

and

$$\begin{bmatrix}0 & \rho_1 v_{qS2}\\ \rho_1 v_{qS1} & 0\end{bmatrix}(\mathbf{i}-\mathbf{r}) = \underset{\sim}{\mathbf{C}}(\Delta\alpha)\begin{bmatrix}0 & \rho_2 v'_{qS2}\\ \rho_2 v'_{qS1} & 0\end{bmatrix}\mathbf{t}. \quad \text{(A-11)}$$

Assuming that the anisotropy is caused by cracking a background matrix rock, the vertical velocity of the split shear wave can be expressed in terms of the background matrix velocity and the degree of anisotropy (Hudson, 1981) as

$$\begin{aligned} v_{qS1} &= v_1, \qquad v_{qS2} = (1-\delta_1)v_1;\\ v'_{qS1} &= v_2, \qquad v'_{qS2} = (1-\delta_2)v_2. \end{aligned} \quad \text{(A-12)}$$

Substituting equation (A-12) into equations (A-10) and (A-11), and simplifying gives

$$\mathbf{r} = \underset{\sim}{\mathbf{R}}\mathbf{i} = \left(\underset{\sim}{\mathbf{X}}_1^{-1}\underset{\sim}{\mathbf{X}}_2 - \underset{\sim}{\mathbf{Y}}_1^{-1}\underset{\sim}{\mathbf{Y}}_2\right)\left(\underset{\sim}{\mathbf{X}}_1^{-1}\underset{\sim}{\mathbf{X}}_2 + \underset{\sim}{\mathbf{Y}}_1^{-1}\underset{\sim}{\mathbf{Y}}_2\right)^{-1}\mathbf{i}, \quad \text{(A-13)}$$

which leads to equation (16) for the reflection coefficients $\underset{\sim}{\mathbf{R}}$.

APPENDIX B
DERIVATION OF APPROXIMATE EQUATION (26)

Small variation of $\Delta\alpha$

First consider the case of small $\Delta\alpha$ variation. Rewrite equation (25) for a more general case,

$$\underset{\sim}{\Lambda}_U(\omega) = \underset{\sim}{\Lambda}_D(\omega) = \begin{bmatrix}\lambda_1 & 0\\ 0 & \lambda_2\end{bmatrix} = \underset{\sim}{\Lambda}(\omega), \quad \text{(B-1)}$$

where λ_1 and λ_2 are, respectively, the phase propagators for the fast and slower split shear waves. Thus,

$$\begin{aligned} &\underset{\sim}{\Lambda}(\omega)\underset{\sim}{\mathbf{C}}(\Delta\alpha)\\ &= \underset{\sim}{\mathbf{C}}(\Delta\alpha)\underset{\sim}{\Lambda}(\omega) + (\lambda_1-\lambda_2)\sin\Delta\alpha\begin{bmatrix}0 & 1\\ 1 & 0\end{bmatrix}\\ &= \underset{\sim}{\mathbf{C}}(\Delta\alpha)\left[\underset{\sim}{\Lambda}(\omega) + (\lambda_1-\lambda_2)\underset{\sim}{\mathbf{C}}^T(\Delta\alpha)\sin\Delta\alpha\begin{bmatrix}0 & 1\\ 1 & 0\end{bmatrix}\right]. \end{aligned} \quad \text{(B-2)}$$

Noting that $\Delta\alpha$ is small, we may approximate:

$$\underset{\sim}{\mathbf{C}}^T(\Delta\alpha)\sin\Delta\alpha = \frac{1}{2}\sin 2\Delta\alpha\begin{bmatrix}1 & 0\\ 0 & 1\end{bmatrix}. \quad \text{(B-3)}$$

Substituting equation (B-3) into equation (B-2) yields,

$$\begin{aligned} &\underset{\sim}{\Lambda}(\omega)\underset{\sim}{\mathbf{C}}(\Delta\alpha)\\ &= \underset{\sim}{\mathbf{C}}(\Delta\alpha)\left[\underset{\sim}{\Lambda}(\omega) + \frac{1}{2}(\lambda_1-\lambda_2)\sin 2\Delta\alpha\begin{bmatrix}0 & 1\\ 1 & 0\end{bmatrix}\right]\\ &= \underset{\sim}{\mathbf{C}}(\Delta\alpha)\left[\underset{\sim}{\Lambda}(\omega) + \begin{bmatrix}0 & \Delta\lambda\\ \Delta\lambda & 0\end{bmatrix}\right], \end{aligned} \quad \text{(B-4)}$$

where,

$$\Delta\lambda = \tfrac{1}{2}(\lambda_1-\lambda_2)\sin 2\Delta\alpha. \quad \text{(B-5)}$$

Similarly,

$$\underset{\sim}{\mathbf{C}}^T(\Delta\alpha)\underset{\sim}{\Lambda}(\omega) = \left[\underset{\sim}{\Lambda}(\omega) + \begin{bmatrix}0 & \Delta\lambda\\ \Delta\lambda & 0\end{bmatrix}\right]\underset{\sim}{\mathbf{C}}^T(\Delta\alpha). \quad \text{(B-6)}$$

Substituting equations (B-4) and (B-6) into equation (24), and omitting higher order terms of $\Delta\lambda$, yields

$$\underset{\sim}{\mathbf{D}}(\omega) \approx \underset{\sim}{\mathbf{C}}(\alpha_G+\Delta\alpha)\begin{bmatrix}\lambda_1 R_1^{\parallel}\lambda_1 & O(\omega)\\ O(\omega) & \lambda_2 R_2^{\parallel}\lambda_2\end{bmatrix}\underset{\sim}{\mathbf{C}}^T(\alpha_S+\Delta\alpha), \quad \text{(B-7)}$$

where,

$$O(\omega) = \tfrac{1}{2}\left[\lambda_1 R_1^{\parallel}\lambda_1 - \lambda_1 R_1^{\parallel}\lambda_2 + \lambda_2 R_2^{\parallel}\lambda_1 - \lambda_2 R_2^{\parallel}\lambda_2\right]\sin 2\Delta\alpha. \quad \text{(B-8)}$$

Letting

$$QS_1(\omega) = \lambda_1 R_1^{\parallel}\lambda_1; \qquad QS_2(\omega) = \lambda_2 R_2^{\parallel}\lambda_2, \quad \text{(B-9)}$$

and substituting into equation (B-7) gives rise to equation (26).

Variation of $\Delta\alpha$ close to 90°

In this case, letting $\Delta\alpha = \pi/2 - \Delta\beta$, then angle $\Delta\beta$ will be small. We note that

$$\begin{aligned} \underset{\sim}{\mathbf{C}}(\Delta\alpha)\underset{\sim}{\mathbf{R}}_0\underset{\sim}{\mathbf{C}}^T(\Delta\alpha) &= \underset{\sim}{\mathbf{C}}(\Delta\alpha)\begin{bmatrix}R_1^{\perp} & 0\\ 0 & R_2^{\perp}\end{bmatrix}\underset{\sim}{\mathbf{C}}^T(\Delta\alpha)\\ &= \underset{\sim}{\mathbf{C}}(-\Delta\beta)\underset{\sim}{\mathbf{C}}(\pi/2)\begin{bmatrix}R_1^{\perp} & 0\\ 0 & R_2^{\perp}\end{bmatrix}\\ &\quad\times\underset{\sim}{\mathbf{C}}(-\pi/2)\underset{\sim}{\mathbf{C}}^T(-\Delta\beta)\\ &= \underset{\sim}{\mathbf{C}}(-\Delta\beta)\begin{bmatrix}R_2^{\perp} & 0\\ 0 & R_1^{\perp}\end{bmatrix}\underset{\sim}{\mathbf{C}}^T(-\Delta\beta). \end{aligned} \quad \text{(B-10)}$$

Thus, the problem for a $\Delta\alpha$ close to 90° is converted to a problem for angle $\Delta\beta$ close to 0°, which has the same form as equation (24) for a small variation of $\Delta\alpha$. Thus equation (26) is also applicable to this case.

APPENDIX C

POLARIZATION MEASUREMENT BY LINEAR TRANSFORMATION

To examine the polarization measurements, two other linear transforms similar to equation (5) have to be used. Following Li and Crampin (1993a),

$$\begin{bmatrix}\xi(t)\\ \eta(t)\end{bmatrix} = \begin{bmatrix}xx(t) - yy(t)\\ xy(t) + yx(t)\end{bmatrix}. \qquad \text{(C-1)}$$

Applying equation (C-1) into the time-domain equation corresponding to equation (28) and making some manipulations gives

$$\begin{bmatrix}\xi(t)\\ \eta(t)\end{bmatrix} = \underset{\sim}{\mathbf{C}}(2\alpha + 2\Delta\alpha)\begin{bmatrix}qS1(t) - qS2(t)\\ 2o(t)\end{bmatrix}, \qquad \text{(C-2)}$$

where $o(t)$ is the inverse Fourier transform of $O(\omega)$ defined by equation (B-8), which is very small compared with the principal time series $qS1(t)$, and $qS2(t)$, as implied by equation (B-8). Thus the direction of the major axis of motion (ξ, η) will be close to $2(\alpha + \Delta\alpha)$.